Available online at www.sciencedirect.com
SCIENCE DIRECT
ELSEVIER
Journal of the European Ceramic Society 26 (2006) 2699–2705
ECERS
www.elsevier.com/locate/jeurceramsoc

Piezo-spectroscopic characterization of alumina-aluminium titanate laminates

Goffredo de Portu [a,d], Salvador Bueno [b], Lorenzo Micele [a,d], Carmen Baudin [b,*], Giuseppe Pezzotti [c,d]

[a] *Institute of Science and Technology for Ceramics, ISTEC-CNR, Via Granarolo, 64-48018 Faenza, Italy*
[b] *Instituto de Ceramica y Vidrio, CSIC-Campus de Cantoblanco, Kelsen 5, 28049 Madrid, Spain*
[c] *Ceramic Physics Laboratory, Kyoto Institute of Technology, KIT, Sakyo-ku, Matsugasaki, 606-8585 Kyoto, Japan*
[d] *Research Institute for Nanoscience, RIN, Sakyo-ku, Matsugasaki, 606-8585 Kyoto, Japan*

Received 19 March 2005; received in revised form 30 June 2005; accepted 8 July 2005
Available online 13 September 2005

Abstract

A multilayered alumina-aluminium titanate composite was prepared by a colloidal route from aqueous suspensions. The structure of the laminate was symmetric and constituted of two external Al_2O_3 layers (width $\cong$ 1750 μm), one central Al_2O_3 layer (width $\cong$ 1200 μm) and two intermediate thin (width $\cong$ 315–330 μm) Al_2O_3–Al_2TiO_5 layers.

Additional monolithic materials with the same compositions as those of the layers were fabricated as reference materials. Young's modulus of the monoliths was determined by three point bending. Dilatometry determinations were performed on green specimens, following the same heating and cooling schedules as those used for sintering the laminate, in order to determine the actual dimensional changes on cooling after sintering. The dimensional changes of the sintered specimens on heating and on cooling were also determined. Microscopic distributions of residual stresses were evaluated by fluorescence piezo-spectroscopy, and they revealed the existence of weak tensile and compressive hydrostatic stresses in the aluminium titanate and alumina layers, respectively. The level and sign of these stresses was in good agreement with those predicted based on analysis of the Young's modulus and the dimensional variations during cooling after sintering of the monoliths with the same compositions as those of the layers. Dimensional variations during cooling after sintering were different from those for sintered materials, which presented hysteresis between heating and cooling. In spite of the presence of compressive residual stresses in the external layers of the laminate, strength values of notched samples of the laminated specimens were lower than those for monoliths of the same composition as the external layers.

Keywords: Laminates; Spectroscopy; Thermal expansion; Al_2O_3; Al_2TiO_5

1. Introduction

Alumina (Al_2O_3)–aluminium titanate (Al_2TiO_5) composites can offer improved flaw tolerance and toughness.[1–7] Toughening in this system is originated by the residual stresses developed, during cooling from the sintering temperature, due to the thermal expansion mismatch between alumina ($\alpha_{i25-1000\,^\circ C}$ = average thermal expansion coefficient between 25 and 1000 °C in the axis i, $\alpha_{a25-1000\,^\circ C} = 8.4 \times 10^{-6}\,^\circ C^{-1}$, $\alpha_{c25-1000\,^\circ C} = 9.2 \times 10^{-6}\,^\circ C^{-1}$)[8] and aluminium titanate ($\alpha_{a25-1000\,^\circ C} = 10.9 \times 10^{-6}\,^\circ C^{-1}$, $\alpha_{b25-1000\,^\circ C} = 20.5 \times 10^{-6}\,^\circ C^{-1}$, $\alpha_{c25-1000\,^\circ C} = -2.7 \times 10^{-6}\,^\circ C^{-1}$).[9] As the toughening mechanisms that have been identified in these composites are crack bridging and microcracking,[6,7] toughening is often associated with low strength.

Laminated materials are being investigated as means to combine strength and toughness in ceramic materials.[10] As an example, Russo et al.[11] proposed structures formed by layers of equal compositions, made of mixtures of alumina and aluminium titanate, and dissimilar microstructures. In partic-

* Corresponding author. Tel.: +34 91 7355840; fax: +34 91 7355843.
E-mail address: cbaudin@icv.csic.es (C. Baudin).

0955-2219/$ – see front matter © 2005 Elsevier Ltd. All rights reserved.
doi:10.1016/j.jeurceramsoc.2005.07.060

ular, these authors fabricated a laminate with small grained (≅1–2 μm) and dense external layers with high strength and internal layers with pores and agglomerates. In that system, flaw tolerance was provided by the *R* curve behaviour of the heterogeneous internal layers. The limit of this approach is the difficulty that involves the co-sintering of layers with the same composition and sufficient microstructural differences as to provide significant differences in the mechanical behaviour.

In a previous work,[12] a laminated structure combining external fine grained alumina layers with internal composite layers of alumina +10 vol.% of aluminium titanate was proposed as means to achieve flaw tolerance and high strength. The obtained laminate presented large strain to fracture, as compared to that of the monoliths of the same composition of the constituent layers. Moreover, under the same loading conditions, the load drop of the laminate samples, once fracture was initiated, occurred in step-like form, whereas the monolith failed catastrophically, thus suggesting the occurrence of additional energy consuming processes during fracture. Strength values for the laminate samples were slightly lower (≅10%) than those corresponding to monoliths of the same composition as that of the external layers.

In this work, the residual stresses developed in this structure are investigated both experimentally, by piezo-spectroscopy, and by calculation, using the properties of monolithic materials with the same compositions as those of the layers that constitute the laminate. The effect of the residual stresses on the fracture of notched samples is discussed.

2. Experimental

2.1. Processing and thermal and mechanical characterisation

Monoliths of monophase alumina and alumina +10 vol.% aluminium titanate and, one laminate were manufactured by a colloidal route from aqueous Al_2O_3 and TiO_2 suspensions using the optimum green processing conditions previously established[12,13] and reaction sintering. The structure of the laminate was symmetric and constituted of two external Al_2O_3 layers (width ≅ 1750 μm), one central Al_2O_3 layer (width ≅ 1200 μm) and two intermediate thin (width ≅ 315–330 μm) Al_2O_3–Al_2TiO_5 layers.

The starting powders were commercial α-Al_2O_3 (Condea, HPA05, USA) and anatase-TiO_2 (Merck, 808, Germany). A mixture of Al_2O_3/TiO_2 with 5 wt.% TiO_2 content was used to obtain the Al_2O_3/Al_2TiO_5 composite materials with 10 vol.% Al_2TiO_5 after reaction sintering. The Al_2O_3 as well as the Al_2O_3/TiO_2 powders were dispersed in deionised water by adding 0.5 wt.% (on a dry solids basis) of a carbonic acid based polyelectrolyte (Dolapix CE64, Zschimmer-Schwarz, Germany). The suspensions (50 vol.% solid loading) were ball milled with Al_2O_3 jar and balls during 4h. Plates with 70 mm × 70 mm × 10 mm dimensions were obtained by slip casting, removed from the moulds and dried in air at room temperature for at least 24 h. The layered plates, constituted by two external and one central alumina layers and two intermediate composite layers, were fabricated by alternately casting the suspensions. Casting times were fixed to reach the desired layer thickness considering the casting kinetics and sintering shrinkage of each suspension. The dried blocks were sintered in air in an electrical box furnace (Termiber, Spain) at heating and cooling rates of 2 °C min^{-1}, with 4 h dwell at 1200 °C during heating and 3 h dwell at the maximum temperature, 1550 °C. Small (12 mm × 5 mm × 5 mm) green samples of the monoliths were used for sintering experiments in a differential dilatometer (Setaram, Setsys 16/18, France) with alumina detector. The same sintering schedule used to obtain the final materials was reproduced in order to determine the dimensional variations on cooling.

The monolithic sintered blocks were machined into bars of 25 mm × 2 mm × 2.5 mm for bending tests (three point bending, 20 mm span, 0.5 mm min^{-1}; Microtest, Spain). The stress-strain curves were calculated from the load values and the displacement of the central point of the surface of the samples in tension during the tests, and Young's modulus was determined from the linear part of the curves. Reported Young's modulus values are the average of five measurements and errors are the standard deviations. Additional sintered samples were machined (10 mm × 5 mm × 5 mm) to test in a differential dilatometer (Netzsch, 402 EP, Germany) with quartz detector, up to 850 °C and using heating and cooling rates of 5 °C min^{-1}. The obtained curves were corrected for the system deformation using a standard of quartz.

Samples of 50 mm × 6 mm × 4 mm of the laminates as well as the monoliths were machined for the mechanical and piezo-spectroscopic measurements. For these latter, one of the lateral faces (50 mm × 6 mm) was diamond polished down to 1 μm and finished with colloidal alumina. Mechanical tests were performed using the SENVB method (three point bending, 40 mm span, 0.005 mm min^{-1}; Microtest, Spain). The notches were introduced with a depth at about 870 μm (a/w ≅ 0.4 of the thickness of the external alumina layer in the laminate).

2.2. Basis of piezo-spectroscopic measurements

The stress field distribution along the cross section of the laminated samples was determined by using piezo-spectroscopy (PS) technique related to the characteristic R1, R2 doublet produced by chromophoric fluorescence of Cr^{3+} impurities in Al_2O_3. The principle of relating an observed line shift in a fluorescence spectrum to the state of stress has been described previously by Grabner.[14] When Al_2O_3 is subjected to a stress σ, the change in frequency $\Delta\nu$ in luminescence line is given by the tensorial relationship:

$$\Delta\nu = \tfrac{1}{3}\Pi_{ii}\sigma_{jj} \quad (1)$$

where Π_{ii} is referred to as the PS coefficient (i.e., relating frequency to stress) and σ_{jj} is the first invariant of the stress tensor ($\sigma_{jj}/3$ being normally referred to as the mean normal stress).

In principle, the overall residual stress field is due to different thermal expansion and elastic mismatch between the constituent ceramic phases of the Al_2O_3/Al_2TiO_5 laminate and consists of two separate components: (i) a microscopic stress field deriving from the microstructural scale from grain-to-grain thermal and elastic mismatches between Al_2O_3 and Al_2TiO_5 phases; and (ii) a macroscopic stress field, which is established to fulfil equilibrium conditions between adjacent layers. To measure merely the second contribution of the stress, data were analyzed following the approach suggested by De Portu et al.[15] for monolithic composites with no laminated structure. These authors established the influence of the ratio matrix/secondary-phase in the determined zero-stress position of the R1 peak as well as of the piezo-spectroscopic coefficient. Moreover, they demonstrated that the average uniaxial PS coefficient, Π_{UNI}, characterizing the linear dependence of the peak shift on stress, strongly depends on many factors specific of the material, especially in processing derived parameters such as grain size, presence of other phases, porosity, etc. Hence, in order to obtain a fluorescence spectra and piezo-spectroscopic coefficient, which takes into account the effect of the microstructure on the stress field before lamination, a preliminary calibration procedure is required case by case for determining the Π_{UNI} value pertinent to each material. For this reason, the frequencies used as a standard value for the stress-free material were collected on monolithic Al_2O_3 and composite Al_2O_3/Al_2TiO_5 bars prepared following the same processing as that of the multilayered specimens. In this way the R1 peak of each stress free material can be precisely obtained and compared with that of the same composition in the laminated structure. Moreover, calibration of spectral shift as a function of externally applied load for each composition was done, according to the procedures described in Section 3.1. Using Eq. (1) the PS coefficient Π_{ii} for both pure alumina and, for the first time, for alumina-aluminium titanate composites were obtained.

2.3. Determination of the residual stresses

To collect fluorescence spectra, the spectrometer apparatus (ISA, T 64000 Jovin-Yvon) employed in the present experiments used, as excitation source, an argon-ion laser operating at a wavelength of 488 nm with a power of 400 mW. For obtaining micron-scale magnification, an optical microscope lens was used both to focus the laser on the sample and to collect the scattered signal. Scattered frequencies were analyzed with a triple monochromator equipped with a charge coupled device (CCD) camera. When focussed by an optical microscope, the dimension of the laser spot on the samples was 5 μm (i.e., using a ×20 optical lens). Thermal and instrumental fluctuations were compensated by monitoring the spectrum using a Hg/Ne discharge lamp. The recorded spectra were analysed with a commercial software (LabSpec 4.02, Horiba/Jobin-Ivon). The frequency shifts were obtained by subtracting from the centre of the peak recorded under stress, the centre frequency of the peak obtained in the unstressed state.

Microscopic stress distributions were measured by collecting linear profiles of spectra on the specimen cross-sections. The automatically collected profiles of spectra were 10 μm-spaced. Specimens were placed on a mapping device (lateral resolution of 0.1 μm), which was connected to a personal computer to drive highly precise displacements (along both X and Y axes) on the specimen surface.

Under the assumption that composites prepared according to the above mentioned process are polycrystalline and without any significant texture, the average component of the hydrostatic stress, $\langle\sigma\rangle=(\sigma_{11}+\sigma_{22}+\sigma_{33})/3$, is calculated by rearranging Eq. (1) as follows:[16]

$$\langle\sigma\rangle = \frac{\Delta\nu}{3\langle\Pi\rangle_{\mathrm{UNI}}} \tag{2}$$

where $\langle\Pi\rangle_{\mathrm{UNI}}$ represents the PS coefficient that is determined from a calibration where the stress is uniaxial. It is important to emphasize that Eq. (2) provides the average hydrostatic stress that is experienced by the phase that generates the spectroscopic signal for which the shift $\Delta\nu$ is monitored. In fact, in laminated structures, far away from external edges,[17] the residual stress field can be considered to be of a biaxial nature; accordingly, it should be computed as 2/3 σ_{ij}. On the other hand, nearby the edges the residual stress field is typically three-dimensional, thus requiring the use of a mean normal stress σ_{jj} in Eq.(1). For stress measurement, R1 band was used in order to avoid errors in fitting due to the superposition of a line of reference Hg/Ne lamp spectrum with R2 band. In relation to the weak deviation from linearity of R1 calibration line evidenced by Ma et al.,[16] considered the high correlation coefficient obtained by lines referred to laminated material and the low stress measured, it was supposed to be negligible.

3. Results and discussion

3.1. Determination of the residual stresses

Unstressed peak position was obtained acquiring an array of 100 spectra on the surface of unstressed reference bars and averaging all the values of the peak centre. For the evaluation of PS coefficient, bending bars of both composites were mounted on a four-point bending jig and loaded with a known load below fracture stress; after the load was applied, the whole jig was moved under the microscope and spectra recorded every 40 μm from the compressive towards the tensile side of the specimen. To reduce the scattering of data, and consequently improve PS coefficient determination, the calibration was repeated three times and the values obtained were averaged. The load was then converted to stress, σ, using

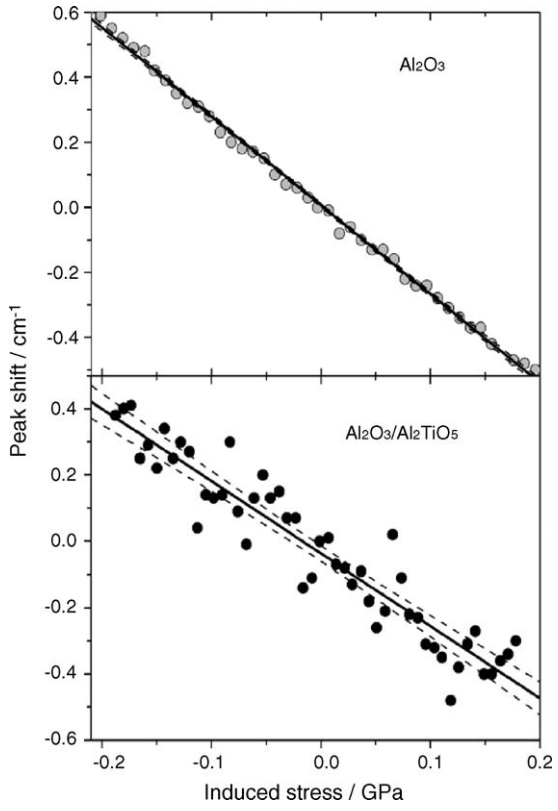

Fig. 1. Stress dependence of the position of R1 band in the materials analyzed in this work: Al_2O_3 (top) and Al_2O_3/Al_2TiO_5 composite (bottom).

the standard four-point-bending elastic equation and the peak shift, $\Delta\nu$, plotted as a function of the applied stress (Fig. 1). The average Π_{UNI} was obtained from the slope of the straight line σ versus $\Delta\nu$. Table 1 summarizes the values of salient piezo-spectroscopic characteristics of the materials studied in the present investigation. Significant diversity was evidenced in data scattering between the pure alumina and the alumina-aluminum titanate composite: in the latter, data were more spread and, consequently, the correlation between peak shift and induced stress was lower. The higher scattering in the composite can be attributed to the effect of residual stresses at the microscopic level on the stress state of the specimen (Section 2.2). In fact, as Al_2TiO_5 is an extremely anisotropic phase in terms of thermal expansion,[9] microscopic residual stresses are expected in the Al_2O_3/Al_2TiO_5 composites, as discussed in the introduction. The level and, moreover, the sign of such stresses would depend on the particular grain to grain orientation, leading to the high scatter observed (Fig. 1, Table 1).

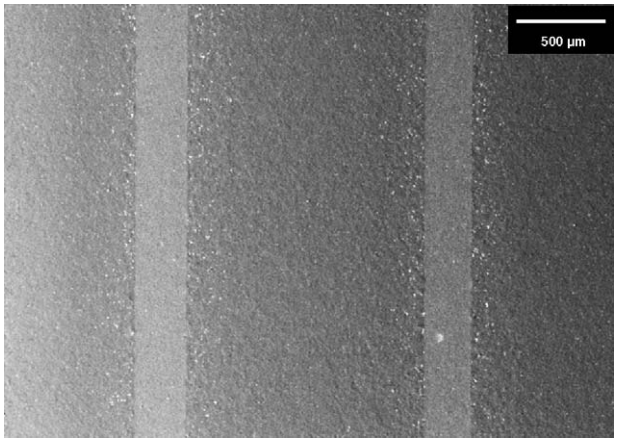

Fig. 2. Structure of the laminate: two thick (1750 μm) external Al_2O_3 layers, observed partially in the figure, one central Al_2O_3 layer (1200 μm) and two intermediate thin (315–330 μm) Al_2O_3–Al_2TiO_5 layers. Scanning electron micrograph of a polished surface (thermally etched, 1500 °C −2 min): Al_2O_3 (dark grey) Al_2O_3-Al_2TiO_5 (clear grey).

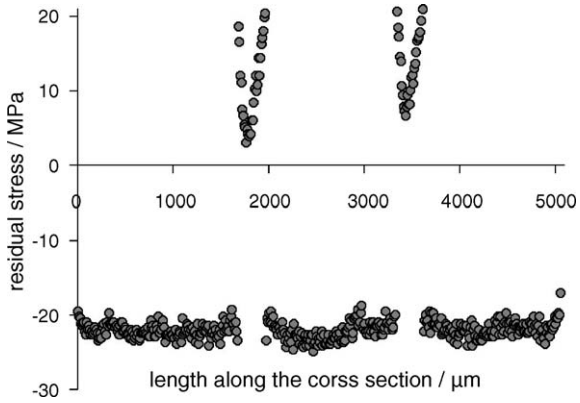

Fig. 3. Profiles of macroscopic residual stress along the cross section. Pure Al_2O_3 layers were in compression, whereas Al_2O_3/Al_2TiO_5 composite layers underwent tensile stresses. The error for residual stress value was ±2 MPa for the alumina layers and ±4 MPa for the composite layers.

Fig. 2 shows the structure of the obtained symmetric laminate. It was constituted of two thick (1750 μm) external Al_2O_3 layers and one central Al_2O_3 layer (1200 μm) and two intermediate thin (315–330 μm) Al_2O_3–Al_2TiO_5 layers.

The macroscopic residual stress profile along the cross section determined using Eq. (2) is plotted in Fig. 3. Results are the average of five profiles collected along the cross section to reduce the scattering of data and to verify the uniformity of residual stress field. In this way, the errors relative to stress calculation were ±2 and ±4 MPa for the Al_2O_3 and Al_2O_3/Al_2TiO_5 layers, respectively. According this profile,

Table 1
Salient piezo-spectroscopic characteristics of R1 band of the investigated materials

Material	Π_{uni} (cm^{-1}/GPa)	Π_{hydro} (cm^{-1}/GPa)	R^2	Unstressed peak position (cm^{-1})
Al_2O_3	2.73 ± 0.03	8.19 ± 0.09	0.993	14407.31 ± 0.01
Al_2O_3/Al_2TiO_5	2.2 ± 0.1	6.6 ± 0.3	0.90	14407.00 ± 0.01

Confidence intervals of the PS coefficient were calculated with the software Origin 6.0, with a probability of 95%.

the Al_2O_3 layers underwent a constant compressive stress of about 20 MPa, whereas the residual stress distribution in the Al_2O_3/Al_2TiO_5 layers, tensile on the whole, varied considerably through the layer thickness: it was approximately 5 MPa in the centre of the layers and rose up to 20 MPa at the interfaces.

3.2. Properties of the monolith and residual stresses

In a previous work,[18] we determined the thermal expansion of the pure Al_2O_3 and the Al_2O_3/Al_2TiO_5 sintered monoliths during heating, which were coincident with those determined here (Fig. 4). From Fig. 4, average thermal expansion values on heating of 8.2 ± 0.1 and $7.8 \pm 0.1 \times 10^{-6}\,^{\circ}C^{-1}$ are derived for pure Al_2O_3 and the composite, respectively. If these data are used to evaluate the residual stress state in the laminate, the expected sign of the residual stresses would be the opposite of that experimentally determined here, as the layers of pure Al_2O_3, with larger thermal expansion coefficient, would contract more on cooling than the composite layers and thus, the former layers would be in tension in the laminate.[19,20] This apparent contradiction is clarified looking at the cooling part of the dilatometry curves in Fig. 4. They are coincident for Al_2O_3 (Fig. 4a) whereas they present an hystheresis from about 700 °C for the composite (Fig. 4b), similar to that reported elsewhere for aluminium titanate based materials.[21] The presence of the hysteresis in the curve corresponding to the composite, does not allow the evaluation of the residual stresses from the standard thermal expansion analysis on heating.

In order to evaluate the actual differences between the dimensional variations of the different layers during cooling, the corresponding part of the sintering curves shown in Fig. 5a were analysed. In alumina based materials, deformation mismatch at temperatures higher than 1200 °C can be accomodated by diffusion,[22] whereas, from 1200 °C to room temperature, this mismatch originates stresses. Therefore, in order to evaluate the stress level and sign in the laminate, the differences between the dimensional variations of specimens during cooling from the "stress free" temperature, 1200 °C, were analysed. In Fig. 5b, these variations are plotted toghether for the two monoliths, after correction for coincident dimensions at 1200 °C. In the considered interval of temperatures (1200–50 °C) the shrinkage for the composite ($\cong 10.1 \times 10^{-6}\,^{\circ}C^{-1}$) is slightly larger than that of Al_2O_3 ($\cong 9.8 \times 10^{-6}\,^{\circ}C^{-1}$), which would imply compressive and tensile residual stresses in the alumina and in the compos-

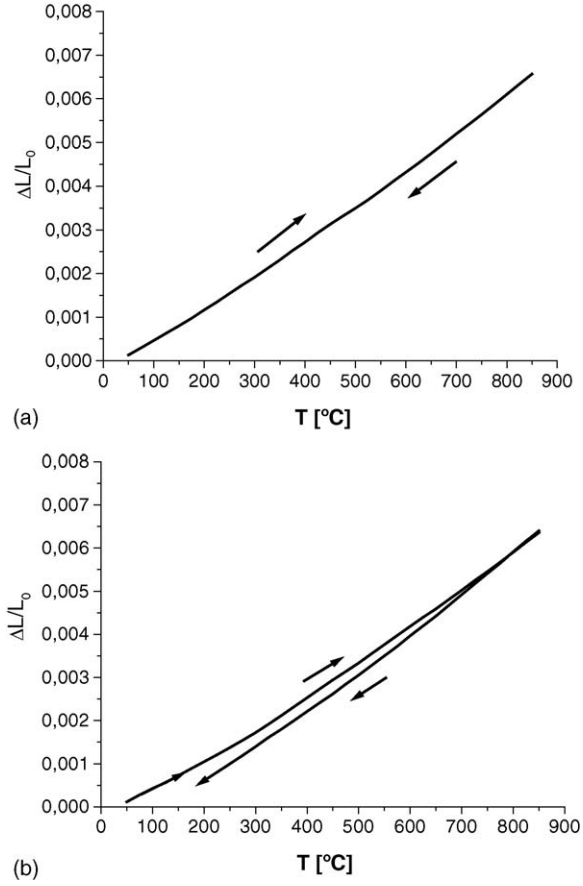

Fig. 4. Dilatometric curves ($\Delta L/L_0$ = length variation) on heating and cooling of the sintered monoliths: (a) Al_2O_3; (b) Al_2O_3 + 10 vol.% Al_2TiO_5.

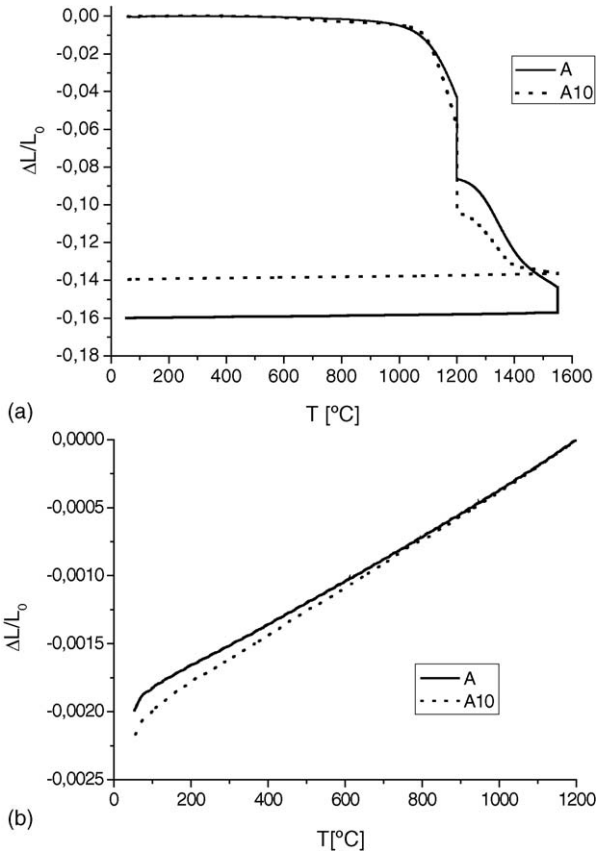

Fig. 5. Dilatometric curves ($\Delta L/L_0$ = length variation) for green compacts of the two studied monoliths heat treated following the sintering schedule. A: Al_2O_3; A10: Al_2O_3 + 10 vol.% Al_2TiO_5. (a) Complete thermal cycle. (b) Cooling from 1200 °C, after correction for coincident dimensions at 1200 °C and apparatus deformation.

ite layers, respectively, as determined by piezo-spectroscopy (Fig. 3).

Appart from differences in the dimensional variations of the different layers during cooling from the sintering temperature, the residual stresses in a laminate are determined by the elastic properties of the constituent layers. Young's modulus of composite materials are usually dependent on the method used for the determination. In general, the stiffer phase dominates over the obtained value when dynamic methods are used whereas static methods are more sensitive to grain boundary characteristics and microscopic residual stresses. These differences are due to the characteristics of the deformations involved in each case, small and instantaneous in the dynamic case and larger and distributed in time in the static case. From Fig. 5b and the discussion above, the expected difference between the dimensional variations of the layers on cooling is 2×10^{-4} in the studied laminate, which is of the same order as strains involved in bending tests ($\sim 10^{-4}$). Consequently, the values of static Young's modulus determined in bending were chosen in this work. Young's modulus for the pure Al_2O_3 monolith, 376 ± 6 GPa, was larger than that for the Al_2O_3–Al_2TiO_5, 272 ± 10 GPa. The fact that residual stresses decreased at the centre of the composite layers, which has also been observed in Al_2O_3–ZrO_2 laminated composites[15,23] can be attributed to the lower elastic modulus of Al_2O_3–Al_2TiO_5 compared to pure Al_2O_3.

The level and sign of the expected residual stresses within symmetrical laminate can be evaluated using simplified model of symmetric plate constituted by alternate layers of the same thickness having a uniform biaxial distribution of stresses across each layer.[19] Using this approach, the arising residual stresses at the centre of the pure Al_2O_3, A, and the composite layers, A10, are given by:

$$\sigma_A = -\frac{\Delta\varepsilon E'_A}{1 + (E'_A n_A h_A / E'_{A10} n_{A10} h_{A10})} \quad (3)$$

$$\sigma_{A10} = -\sigma_A \frac{n_A}{n_{A10}} \frac{h_A}{h_{A10}} \quad (4)$$

where $\Delta\varepsilon$ is the thermal expansion mismatch between the layers, $n_{A,A10}$ and $h_{A,A10}$ are the number and thickness of the layers, respectively, and $E'_{A,A10}$ is equal to $E_{A,A10}/(1-\nu)$ where $E_{A,A10}$ is the Young's modulus and ν is the Poisson's ratio. Assuming the same width for the three Al_2O_3 layers as that of the central one in the laminate studied here and using for $\Delta\varepsilon$ the value derived from the cooling part of the sintering curves (2×10^{-4}, Fig. 5b) compressive stress at the centre of the central alumina layer of about 9 MPa and tensile stresses of about 48 MPa at the centres of the composite layers, which are in reasonable agreement with the experimental values (Fig. 3), are obtained. Differences would be in part due to the "edge effect" discussed elsewhere:[17] briefly, near edges the residual stress state is not biaxial, because the edges themselves must be traction free. For that reason, the actual stress state is the superimposition of the bulk residual stress and another component opposite to the first one, which reduces the overall residual stress in the superficial region investigated by piezo-spectroscopy.

The notch entered 870 μm in both, the laminate and the monolith, which corresponded to ≅0.4 the thickness of the first layer in the laminate. Strength values of the notched samples calculated using the approach by Timoshenko for stress through a laminated structure[24] were 91±3 MPa for the laminate and 104±5 MPa for the monolith, thus, following the same trend (≅10% lower for the laminate) as that previously observed in un-notched samples.[12] This strength decrease in the laminate, in spite of the compressive residual stresses existing in the external alumina layer of the laminate, where the whole notch was located, might be related with the lower stiffness of the laminate as compared to the pure Al_2O_3 monolith, due to the lower modulus of the composite layers and the microstructural characteristics of the interfaces between chemically incompatible layers.[18]

4. Conclusions

It has been possible to determine the microscopic distributions of residual stresses developed in a laminate, constituted by thick external (≅1750 μm) and central (≅1200 μm) alumina layers and thin (≅320 μm) intermediate alumina +10 vol.% aluminium titanate layers, by fluorescence piezo-spectroscopy. Weak tensile and compressive hydrostatic stresses in the aluminium titanate and alumina layers, respectively, have been detected. The level and sign of these stresses is in good agreement with those expected from the Young's modulus and the actual dimensional variations experienced by the constituent layers on cooling after sintering.

Acknowledgements

Work supported in part by the European Community's Human Potential Programme under contract HPRN-CT-2002-00203 [SICMAC]. The Spanish authors acknowledge the support of the projects CICYT MAT 2003-00836 and CAM, GRMAT0707-2004 and the grant CSIC I3P-BPD2001-1 (Spain). G. de Portu is grateful to Japan Society for the Promotion of Science (JSPS) and Italian National Research Council (CNR) for the financial support to his work in Japan. The contribution of Italian Ministry for Foreign Affair (MAE), which supported the creation of RIN is also gratefully acknowledged.

References

1. Runyan, J. L. and Bennison, S. J., Fabrication of flaw-tolerant aluminum-titanate-reinforced alumina. *J. Eur. Ceram. Soc.*, 1991, **7**, 93–99.
2. Padture, N. P., Bennison, S. J. and Chan, H. M., Flaw-tolerance and crack-resistance properties of alumina-aluminium titanate composites with tailored microstructures. *J. Am. Ceram. Soc.*, 1993, **76**, 2312–2320.

3. Bartolomé, J., Requena, J., Moya, J. S., Li, M. and Guiu, F., Cyclic fatigue crack growth resistance of Al_2O_3–Al_2TiO_5 composites. *Acta Mater.*, 1996, **44**, 1361–1370.
4. Bartolomé, J., Requena, J., Moya, J. S., Li, M. and Guiu, F., Cyclic fatigue of Al_2O_3–Al_2TiO_5 composites in direct push-pull. *Fatigue Fract. Eng. Mater. Struct.*, 1997, **20**, 789–798.
5. Uribe, R. and Baudín, C., Influence of a dispersion of aluminum titanate particles of controlled size on the thermal shock resistance of alumina. *J. Am. Ceram. Soc.*, 2003, **86**, 846–850.
6. Lawn, B. R., Padture, N. P., Braun, L. M. and Bennison, S. J., Model for toughness curves in two-phase ceramics: I, basic fracture mechanics. *J. Am. Ceram. Soc.*, 1993, **76**, 2235–2240.
7. Padture, N. P., Runyan, J. L., Bennison, S. J., Braun, L. M. and Lawn, B. R., Model for toughness curves in two-phase ceramics: II, microstructural variables. *J. Am. Ceram. Soc.*, 1993, **76**, 2241–2247.
8. Taylor, D., Thermal expansion data: III. Sesquioxides, M_2O_3 with the corundum and the A-, B- and C-M_2O_3. *Br. Ceram. Trans. J.*, 1984, **83**, 92–98.
9. Taylor, D., Thermal expansion data. XI. Complex oxides, A_2BO_5, and the garnets. *Br. Ceram. Trans. J.*, 1987, **86**, 1–6.
10. Chan, H. M., Layered ceramics: processing and mechanical behavior. *Annu. Rev. Mater. Sci.*, 1997, **27**, 249–282.
11. Russo, C. J., Harmer, M. P., Chan, H. M. and Miller, G. A., Design of a laminated ceramic composite for improved strength and toughness. *J. Am. Ceram. Soc.*, 1992, **75**, 3396–4000.
12. Bueno, S., Moreno, R. and Baudín, C., Design and processing of Al_2O_3–Al_2TiO_5 layered structures. *J. Eur. Ceram. Soc.*, 2005, **25**, 847–856.
13. Bueno, S., Moreno, R. and Baudín, C., Reaction sintered Al_2O_3/Al_2TiO_5 microcrack-free composites obtained by colloidal filtration. *J. Eur. Ceram. Soc.*, 2004, **24**, 2785–2791.
14. Grabner, L., Spectroscopic technique for the measurement of residual stress in sintered Al_2O_3. *J. Appl. Phys.*, 1978, **49**, 580–583.
15. De Portu, G., Micele, L., Sekiguchi, Y. and Pezzotti, G., Measurement of residual stress distributions in Al_2O_3/3Y-TZP multilayered composites by fluorescence and Raman microprobe piezo-spectroscopy. *Acta Mater.*, 2005, **53**, 1511–1520.
16. Ma, Q. and Clarke, D. R., Stress measurement in single-crystal and polycrystalline ceramics using their optical fluorescence. *J. Am. Ceram. Soc.*, 1993, **76**, 1433–1440.
17. Sergo, V., Lipkin, D. M., De Portu, G. and Clarke, D. R., Edge stresses in alumina/zirconia laminates. *J. Am. Ceram. Soc.*, 1997, **80**, 1633–1638.
18. Bueno, S. and Baudín, C., In situ developed laminates with large microstructural differences between layers of similar composition. *J. Mater. Sci.*, in press.
19. Oel, H. J. and Fréchette, V. D., Stress Distribution in multiphase systems: I, composites with planar interfaces. *J. Am. Ceram. Soc.*, 1967, **50**, 542–549.
20. Ho, S., Hillman, C., Lange, F. F. and Suo, Z., Surface cracking in layers under biaxial, residual compressive stress. *J. Am. Ceram. Soc.*, 1995, **78**, 2353–2359.
21. Hasselman, D. P. H., Donaldson, K. Y., Anderson, E. M. and Johnson, T. A., Effect of thermal history on the thermal diffusivity and thermal expansion of an alumina-aluminium titanate composite. *J. Am. Ceram. Soc.*, 1993, 76.
22. Blendell, J. E. and Coble, R. L., Measurement of stress due to thermal expansion anisotropy in Al_2O_3. *J. Am. Ceram. Soc.*, 1982, **65**(3), 174–178.
23. De Portu, G., Micele, L. and Pezzotti, G., Characterization of delamination cracks in Al_2O_3/Al_2O_3+3Y-TZP multilayered composites by Raman and fluorescence piezo-spectroscopy. *Appl. Spectr.*, 2005, **59**, 21–25.
24. Timoshenko, S. P., *Mechanics of Materials*. VanNostrand Reinhold Co, New York, USA, 1972.